Electronic Raman spectra in superconducting graphene: A probe of the pairing symmetry

Hong-Yan Lu,[1,*] San Chen,[1] Yuehua Xu,[2] Li-Qin Zhang,[1] Da Wang,[3] and Wan-Sheng Wang[4]
[1]*School of Physics and Electronic Information, Huaibei Normal University, Huaibei 235000, China*
[2]*School of Mathematics and Physics, Changzhou University, Changzhou 213164, China*
[3]*Department of Physics, University of California, San Diego, California 92093, USA*
[4]*National Laboratory of Solid State Microstructures, Nanjing University, Nanjing 210093, China*
(Received 19 May 2013; revised manuscript received 23 July 2013; published 14 August 2013)

Motivated by the hot issue of the pairing symmetry of superconducting (SC) graphene, we theoretically study the electronic Raman spectra on a two-dimensional honeycomb lattice with two possible SC pairing symmetries, the $d_{x^2-y^2} + id_{xy}$ wave ($d + id'$ wave) and extended s wave, at half filling and different doping levels. When it is not doped, the Raman spectrum for $d + id'$-wave pairing consists of a low-energy kink and a high-energy Raman peak, while the spectrum for the extended-s-wave pairing is similar to that in the normal state. On the other hand, when it is doped, besides the high-energy Raman peak, a low-energy pair breaking peak arises in both of the two pairings, which is forbidden in the otherwise normal state graphene at the same doping level. For the Raman spectrum of $d + id'$-wave pairing, there is an energy cutoff at low energy, below which no Raman absorption is allowed, indicating a full gap. While for the extended-s-wave pairing, with the increasing of the doping level, the low energy Raman behavior changes from a linear line to the appearance of cutoff energy, indicating that the gap changes from nodal to full. Therefore, we propose that the distinct features of Raman spectra can be used to differentiate the two pairings of SC graphene.

DOI: 10.1103/PhysRevB.88.085416 PACS number(s): 74.20.Rp, 74.25.Jb, 74.25.Gz, 73.22.Pr

I. INTRODUCTION

Graphene, first isolated by Novoselov and Geim,[1] is a two-dimensional electronic system on a honeycomb lattice with its electronic excitations being described by linear dispersing Dirac fermions. It has attracted lots of attention in the condensed matter community.[2,3] One of the intriguing properties of graphene is that the chemical potential can be tuned by chemical doping[4] or electrolytic gating;[5] therefore it is possible to change the type of carriers (electrons or holes) and dope graphene far away from the Dirac point. In particular, the carrier density can be tuned to the vicinity of the van Hove singularities (VHSs) in the band structure,[4] which occur at 1/4 electron or hole doping. Doped graphene has a finite density of state at the Fermi level, which, combined with the antiferromagnetic spin fluctuations around half filling,[6,7] may lead to unusual superconductivity. Experimentally, superconducting (SC) states have been realized in graphene by the proximity effect through contact with SC electrodes,[8–10] indicating that Cooper pairs can propagate coherently in graphene. In addition, first principles calculations suggest that superconductivity in graphene could be induced by sulfur absorption[11] or lithium deposition.[12]

To understand the superconductivity of graphene, various theoretical researches have been done. Uchoa and Castro Neto[13] suggested that an extended-s-wave superconductor with spin singlet bond pairing may be realized at the mean-field level with possible phonon- or plasma-mediated mechanisms. While in the strong correlation scenario with the well-known resonant-valence-bond (RVB) pairing picture, Black-Schaffer and Doniach[11] found a SC state with $d_{x^2-y^2} + id_{xy}$ ($d + id'$) symmetry to be the lowest energy state in the mean-field theory, which is similar to the SC state in the triangular lattice.[14,15] The $d + id'$-wave SC state is interesting in that it is topologically nontrivial and breaks the time reversal symmetry. This pairing symmetry is also supported by the functional renormalization group (FRG) method with on-site and nearest-neighbor interacting terms[16] and extensive variational Monte Carlo (VMC) simulations of the repulsive Hubbard model[17] when graphene is doped away from half filling. Besides, the $d + id'$-wave SC state of graphene can be obtained from the quantum Monte Carlo (QMC) simulations of the extended Hubbard model close to half filling.[18] When it is doped near the VHSs (at 1/4 doping), renormalization group (RG),[19] FRG,[20,21] and VMC[20] methods all support the $d + id'$ pairing.

Regardless of the microscopic mechanism, the determination of the pairing symmetry of SC graphene, both theoretically and experimentally, is highly desirable. In this paper, we try to figure out a method to differentiate the novel $d + id'$-wave symmetry from the extended-s-wave symmetry. Jiang *et al.*[22] calculated the Andreev conductance spectra through a normal/SC graphene structure, which show different behaviors for the two symmetries and can be used to discern them. Here, we determine to use electronic Raman scattering as an additional but important probe for the pairing symmetry. The electron Raman response has been applied successfully for detecting the pairing symmetry of cuprate superconductors[23] and iron-based superconductors.[24] It is, therefore, natural to explore how it can be applied to SC graphene.

In this paper, using a tight-binding model within the mean-field approximation[11,22] and the standard Green function method, we study theoretically the electronic Raman spectra on a two-dimensional honeycomb lattice with $d + id'$-wave and extended-s-wave pairing symmetries at half filling and away from half filling. We find that the electronic Raman spectra for each pairing symmetry behave differently when the doping level changes. At the same doping level, the Raman spectra for the two parings are also different. At the half filling, the Raman spectrum for $d + id'$ wave shows a low-energy kink and a high-energy Raman peak, while for the extended s wave, the Raman spectrum is similar to that in the normal state. When doped away from half filling, there is a low-energy pair

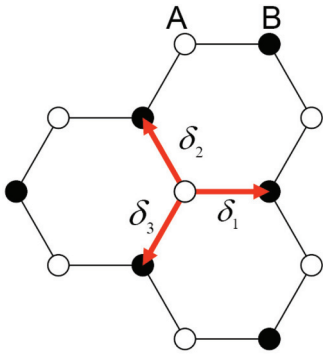

FIG. 1. (Color online) Honeycomb lattice structure of graphene consisting of two sublattices labeled as A and B. δ_α ($\alpha = 1,2,3$) are the nearest-neighbor vectors, which are denoted by red arrows.

breaking peak and a high-energy Raman peak. The position of Raman peaks and the low-energy Raman behavior are different for the two pairings; therefore they can be used to distinctively discern them.

II. MODEL AND METHODS

Graphene consists of two sublattices labeled as A and B, as shown in Fig. 1. Here we consider the SC pairing between the two sublattices; then the mean-field Hamiltonian can be written in reciprocal space as follows:[11,17]

$$H = \sum_{\mathbf{k}\sigma}[f(\mathbf{k})a^\dagger_{\mathbf{k}\sigma}b_{\mathbf{k}\sigma} + \text{H.c.}] - \mu\sum_{\mathbf{k}\sigma}(a^\dagger_{\mathbf{k}\sigma}a_{\mathbf{k}\sigma} + b^\dagger_{\mathbf{k}\sigma}b_{\mathbf{k}\sigma}) - \sum_{\mathbf{k}}[\Delta(\mathbf{k})(a^\dagger_{\mathbf{k}\uparrow}b^\dagger_{-\mathbf{k}\downarrow} - a^\dagger_{\mathbf{k}\downarrow}b^\dagger_{-\mathbf{k}\uparrow}) + \text{H.c.}], \quad (1)$$

where $a^\dagger_{\mathbf{k}\sigma}$ and $b^\dagger_{\mathbf{k}\sigma}$ are electron creation operators on A and B sublattices with momentum $\mathbf{k}$ and spin σ, μ is the chemical potential, and $f(\mathbf{k})$ is the free electron dispersion and can be written as $f(\mathbf{k}) = -t\sum_\alpha e^{i\mathbf{k}\cdot\boldsymbol{\delta}_\alpha}$ with $\boldsymbol{\delta}_\alpha$ ($\alpha = 1,2,3$) being vectors that go from an A site to the three nearest B sites as seen in Fig. 1. t is the hopping energy between nearest neighbors. The SC gap function is $\Delta(\mathbf{k}) = \sum_\alpha \Delta_{\boldsymbol{\delta}_\alpha}e^{i\mathbf{k}\cdot\boldsymbol{\delta}_\alpha}$. For the extended-$s$-wave pairing, $\Delta_{\boldsymbol{\delta}_\alpha} = \Delta$, where Δ is the pairing strength. While for the $d + id'$-wave pairing, the mean-field solution provides $\Delta_{\boldsymbol{\delta}_\alpha} = \Delta e^{i2\pi(\alpha-1)/3}$ ($\alpha = 1,2,3$).[11] In our calculations, we use t as the unit of energy, and set $\Delta = 0.1t$.

For convenience, we rewrite the Hamiltonian as $H = \sum_{\mathbf{k}}\Psi^\dagger_{\mathbf{k}}h_{\mathbf{k}}\Psi_{\mathbf{k}}$, where $\Psi_{\mathbf{k}} = (a_{\mathbf{k}\uparrow},b_{\mathbf{k}\uparrow},a^\dagger_{-\mathbf{k}\downarrow},b^\dagger_{-\mathbf{k}\downarrow})^T$ is the Nambu spinor and $h_{\mathbf{k}}$ is a 4×4 Hermitian matrix associated with the SC Hamiltonian,

$$h_{\mathbf{k}} = \begin{pmatrix} -\mu & f(\mathbf{k}) & 0 & -\Delta(\mathbf{k}) \\ f(\mathbf{k})^* & -\mu & -\Delta(-\mathbf{k}) & 0 \\ 0 & -\Delta(-\mathbf{k})^* & \mu & -f(-\mathbf{k})^* \\ -\Delta(\mathbf{k})^* & 0 & -f(-\mathbf{k}) & \mu \end{pmatrix}. \quad (2)$$

By diagonalizing $h_{\mathbf{k}}$, we can obtain the eigenvalues $E_{\mathbf{k},m}$ ($m = 1,2,3,4$) and the corresponding eigenvectors $|\mathbf{k},m\rangle$. Then the Matsubara Green function $G(\mathbf{k},i\omega_n)$ [$\omega_n = (2n+1)\pi T$ is the Matsubara frequency with T the temperature] can be written in the form of 4×4 matrix as

$$G(\mathbf{k},i\omega_n) = \sum_{m=1}^{4}\frac{|\mathbf{k},m\rangle\langle\mathbf{k},m|}{i\omega_n - E_{\mathbf{k},m}}, \quad (3)$$

which forms the basis for further calculations.

Next, we calculate the electronic Raman spectra for SC graphene. The electronic Raman scattering measures the fluctuations of the effective density operator $\rho_{\mathbf{q}} = \sum_{\mathbf{k}\sigma}\gamma_{\mathbf{k}}C^\dagger_{\mathbf{k}+\mathbf{q}\sigma}C_{\mathbf{k}\sigma}$ in the limit of $\mathbf{q}\to 0$. Here $\mathbf{q}$ is the momentum transfer from the lights, which is vanishingly small. $\gamma_{\mathbf{k}}$ is the Raman vertex which describes the second-order coupling between electrons and lights. In the case of small momentum transfers and the energy of incident light smaller than the optical band gap, it can be written in terms of the curvature of normal state energy band dispersion.[23] In our case, in the matrix form, it can be written as

$$\gamma_{\mathbf{k}} = (\mathbf{n}_i\cdot\nabla_{\mathbf{k}})(\mathbf{n}_s\cdot\nabla_{\mathbf{k}})h_{\mathbf{k}}|_{\Delta(\mathbf{k})=0}, \quad (4)$$

in which $\mathbf{n}_i$ and $\mathbf{n}_s$ are unit vectors for the polarizations of the incident and scattered lights. The bare electronic Raman response function can be written as[23] $\chi^0_{\gamma\gamma}(i\nu_n) = \int_0^\beta d\tau e^{i\nu_n\tau}\langle T_\tau[\rho_{\mathbf{q}}(\tau)\rho_{-\mathbf{q}}(0)]\rangle$, where T_τ is the complex time τ ordering operator, $\beta = 1/T$ with T the temperature. By further calculations, it can be written as

$$\chi^0_{\gamma\gamma}(i\nu_n) = -\frac{T}{N}\sum_{\mathbf{k},i\omega_n}\text{Tr}[\gamma_{\mathbf{k}}G(\mathbf{k},i\omega_n)\gamma_{\mathbf{k}}G(\mathbf{k},i\omega_n + i\nu_n)], \quad (5)$$

where N is the number of lattice sites, and G is the single particle Green function given above.

The long-range Coulomb interactions between the fluctuating electrons have a screening effect on the electronic Raman scattering. By virtue of the random-phase approximation (RPA), the effect of Coulomb screening on the electronic Raman response function can be written as[23,25,26]

$$\chi_{\gamma\gamma} = \chi^0_{\gamma\gamma} + \frac{\chi^0_{\gamma 1}\chi^0_{1\gamma}}{v_q^{-1} - \chi^0_{11}}, \quad (6)$$

where $\chi^0_{\gamma 1}$ and χ^0_{11} are obtained by replacing one or two momentum-dependent vertices $\gamma_{\mathbf{k}}$ by a constant matrix

$$\begin{pmatrix} 1 & 0 & 0 & 0 \\ 0 & 1 & 0 & 0 \\ 0 & 0 & -1 & 0 \\ 0 & 0 & 0 & -1 \end{pmatrix} \quad (7)$$

in $\chi^0_{\gamma\gamma}$. The -1 terms in the matrix originate from the particle-hole transform. v_q in Eq. (6) is the Fourier transform of the Coulomb interaction and $v_q^{-1}\sim q$ for graphene. In the limit of $q\sim 0$, v_q^{-1} is negligible and the electronic Raman response function can be further written as

$$\chi_{\gamma\gamma} = \chi^0_{\gamma\gamma} - \frac{\chi^0_{\gamma 1}\chi^0_{1\gamma}}{\chi^0_{11}}. \quad (8)$$

The Raman intensity (RI) is finally determined by $-\frac{1}{\pi}\text{Im}\chi_{\gamma\gamma}(i\nu_n\to\omega + i\eta)$, in which ω is the Raman shift.

To better understand the electronic Raman spectra, we also calculate the spectral weight at the Fermi surface (FS) and the density of states (DOS), which could be, respectively, obtained by

$$A(\mathbf{k},\omega=0) = -\frac{1}{\pi}\mathrm{Im}[G_{11}(\mathbf{k},\omega=0) + G_{22}(\mathbf{k},\omega=0) + G_{33}(\mathbf{k},\omega=0) + G_{44}(\mathbf{k},\omega=0)], \quad (9)$$

and

$$\rho(\omega) = -\frac{1}{\pi N}\sum_{\mathbf{k}}\mathrm{Im}[G_{11}(\mathbf{k},\omega+i\eta) + G_{22}(\mathbf{k},\omega+i\eta) + G_{33}(\mathbf{k},-\omega+i\eta) + G_{44}(\mathbf{k},-\omega+i\eta)]. \quad (10)$$

III. RESULTS AND DISCUSSION

We now present and discuss the numerical results. First, we show the amplitude of the gap function in the reciprocal space for $d+id'$-wave and extended-s-wave pairing symmetries, which behave differently and can be seen in Fig. 2. From Fig. 2(a), we can see that the gap amplitude is zero at one Dirac point K, but is at a maximum at the other Dirac point K' for the $d+id'$-wave pairing. While for the extended-s-wave pairing, the amplitude of the gap is zero at both the Dirac points as shown in Fig. 2(b). This difference will lead to different behaviors of SC graphene, such as spectral weight on the FS, DOS, and electronic Raman spectra, which will be shown later.

We have done calculations at half filling ($\mu=0$) and at different electron/hole doping levels. We found that the electronic Raman spectrum for the SC state graphene with a certain pairing symmetry and at a certain doping level is independent of the light polarization configuration. Besides, the Raman spectra are the same for the same doping level, no matter whether it is electron doped or hole doped. These two behaviors of the Raman spectra are the same as those in the normal state graphene.[27] To check our calculations on the SC state graphene, we set the SC pairing strength $\Delta=0$, and found the Raman spectra can return to results of normal state graphene, which partly proves the correctness of our calculations.

Then we show and discuss the results at half filling and two electron doped cases, which, respectively, correspond to chemical potential $\mu=0$, $\mu=0.5t$, and $\mu=t$ (doping to the VHSs). At $\mu=0$, all the results, including spectral weight at the FS, DOS, and Raman spectra for $d+id'$-wave pairing and extended-s-wave pairing can be seen in Fig. 3. For comparison, the DOS and Raman spectra in the normal state are also drawn (in green lines). For the $d+id'$-wave pairing state, by enlarging Fig. 3(a), we find that the FS near K and K' are four points instead of one point in the normal state. Near the K point, one of the four Fermi points is at the K point; the other three points are centered around the K point and along the three Γ-K directions. The FS at K' points can be obtained from that of the K point by revolving 60° around the center of the first BZ. Although the gap for $d+id'$ pairing is different for K and K' points, the FS is similar because of the symmetry between the two sublattices of graphene. Reviewing the amplitude of the gap $|\Delta(\mathbf{k})|$ in Fig. 2(a), we can see that though a gap opens at K', it is zero at the K point. Therefore, the amplitude of the DOS is not zero around $\omega=0$ as seen in Fig. 3(b). To see this more clearly, an inset is plotted, from which we can see that two kinks arise at $\omega=\pm0.3t$ and the DOS at $\omega=0$ is higher than that of the normal state. The kinks originate from the SC pairing gap at K' with the gap amplitude $|\Delta(\mathbf{k})|=0.3t$, which can be seen from the color bar of Fig. 2(a). At the other range of energy, the DOS is the same as that of the

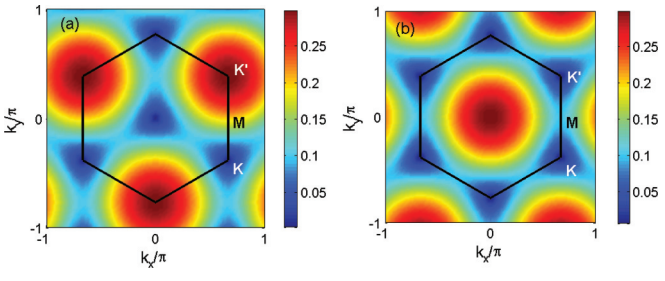

FIG. 2. (Color online) Amplitude of the gap $|\Delta(\mathbf{k})|$ in the reciprocal space for the (a) $d+id'$ wave and (b) extended s wave. Here we set the pairing strength $\Delta=0.1t$. The amplitude can be seen from the color bar. The black hexagons indicate the Brillouin zone (BZ) boundary, with K and K' being Dirac points on the corners of it and the M point at the middle of the K and K' points.

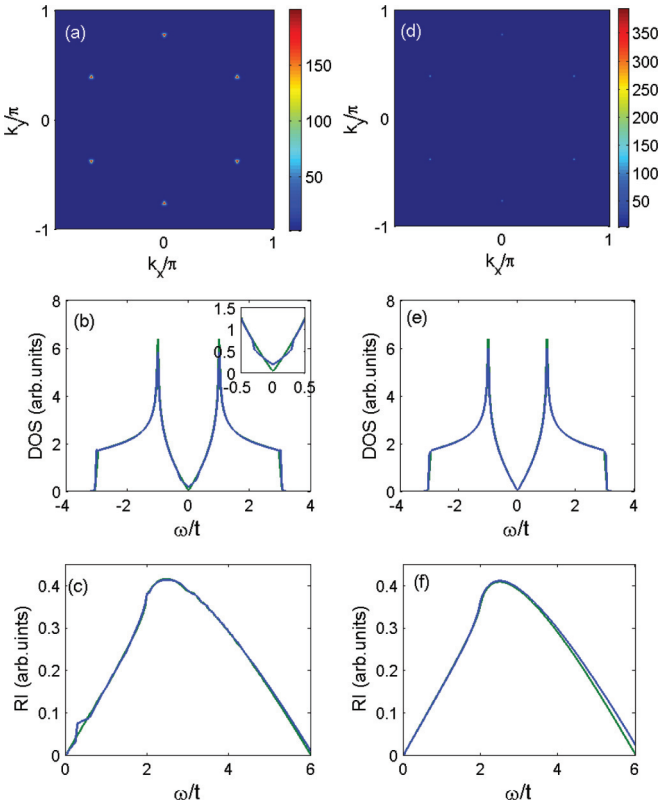

FIG. 3. (Color online) The results for $\mu=0$. (a), (b), and (c), respectively, show spectral weight at the FS, DOS, and Raman spectra (Raman intensity of the screened Raman response function as a function of Raman shift) for $d+id'$-wave pairing. For extended-s-wave pairing, the corresponding results are shown in (d), (e), and (f). In the figures of the DOS and Raman spectra, lines in the color of blue and green, respectively, denote results in the SC state and normal state. In (b), the inset shows the DOS around the Fermi level $\mu=0$. Note that RI in the vertical ordinates of (c) and (f) is an abbreviation for Raman intensity.

normal state graphene. For the electronic Raman spectrum, it is well known that a pair breaking peak (PBP) appears at $\omega = 2|\Delta(\mathbf{k})|$. In this case, a kink arises at around $\omega = 0.6t$ [Fig. 3(c)]. This also originates from the SC pairing gap at K'. At the other range of energy, the Raman absorption comes from the vertical excitations from the valence band to the conduction band. We can see that the Raman intensity is finite and reaches a maximum at $\omega = 2.5t$, which overlaps with the Raman spectrum of normal state graphene.[27] For extended-s-wave pairing, since the gap is zero at the Dirac points [Fig. 2(b)], the FS and DOS at $\mu = 0$ [Figs. 3(d) and 3(e), respectively] are the same as those of the normal state graphene. For the Raman spectrum [Fig. 3(f)], it also follows that of the normal state except that the intensity is a little higher at high energy. As is known, the position of the Raman peak (Raman shift) is more meaningful, from which we can obtain the information of the SC gap or quasiparticle excitation gap. Therefore, the small difference of Raman intensity between the SC state and normal state can be ignored. From the results above, we can see that the Raman spectra are different for the two pairings at $\mu = 0$, but since the Raman spectrum for extended-s-wave pairing can not be easily distinguished from the normal state one, more features of the spectra are needed. We then show Raman spectra for the two pairings in doping cases.

At $\mu = 0.5t$, the results are shown in Fig. 4. The FS of normal state graphene at this doping level is six near-triangles centered at the six Dirac points (not shown here). While for the SC state graphene, the SC gap opens on the FS. For the $d + id'$-wave pairing, Fig. 4(a) shows that the gap on the near-triangle is anisotropic. While for the extended-s-wave pairing, Fig. 4(d) shows that the gap is isotropic. These are understandable by comparing the shape of the FS and the amplitude of the gap on it in Fig. 2. The opening of the gap on the FS for the two pairings can also be seen from the DOS in Figs. 4(b) and 4(e). For the $d + id'$-wave pairing, the amplitude of the DOS is nearly zero for $-0.1t < \omega < 0.1t$ and can be viewed as a full gap. For the Raman spectrum [Fig. 4(c)], it follows that of the normal state at $\omega > t$. Below $\omega = t$, where Raman absorption is forbidden in the normal state, a PBP arises in the SC graphene with $d + id'$-wave pairing. Particularly, for $\omega < 0.2t$, there is also no Raman absorption, indicating the SC gap is full. While for the extended-s-wave pairing, the DOS is zero only at $\omega = 0$ [Fig. 4(e)], and, therefore, can be viewed as a nodal gap. This leads to a linear Raman spectrum at low energy as shown in Fig. 4(f). In this figure, Raman absorption is forbidden at $0.5t < \omega < t$, which can be understood from the fact that besides the SC pair breaking Raman peak, the zero-momentum interband particle-hole excitation needs a threshold energy 2μ (equals to t here), below which there is no phase space for the excitation. For $\omega > t$, the Raman spectrum is the same as that of the normal state graphene at $\mu = 0.5t$. From these results, we can see that the Raman spectrum for SC graphene with the two pairings behaves differently at $\mu = 0.5t$ and can be used to discern them.

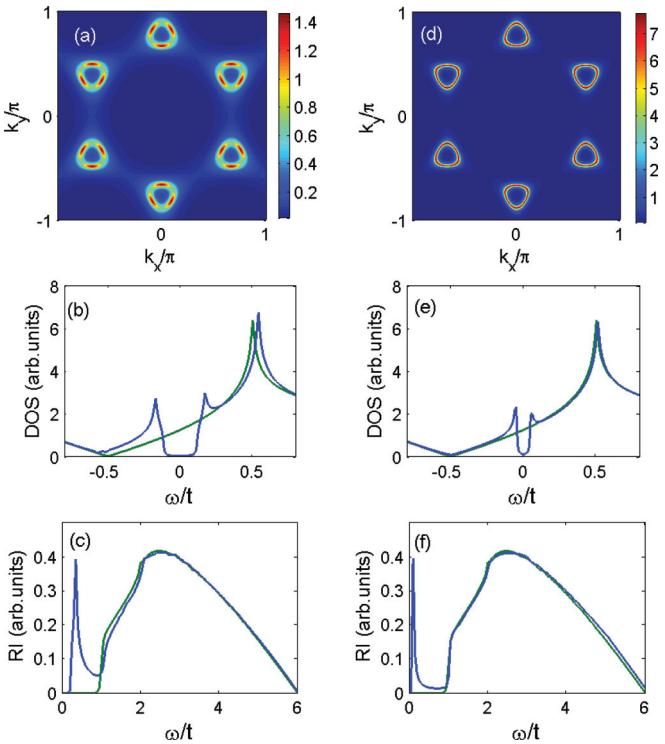

FIG. 4. (Color online) The same plot as Fig. 3 but for $\mu = 0.5t$. For the DOS in (b) and (e), only the results around the Fermi level are shown.

At $\mu = t$, it is doped to the VHSs. The FS in the first BZ for the normal state graphene is a hexagon with the vertices located at M points which is labeled in Fig. 2. For the SC state, a gap opens on the FS, which can be seen in Figs. 5(a) and 5(d) for $d + id'$- and extended-s-wave pairings, respectively. From the DOS in Figs. 5(b) and 5(e), we can see that the gaps at the FS are full for both of the two pairings. For the $d + id'$-wave pairing, the DOS is zero at $-0.1t < \omega < 0.1t$, and two van Hove singularity peaks arise at $\omega = \pm 0.2t$, leading to a Raman peak at $\omega = 0.4t$ and an energy cutoff at

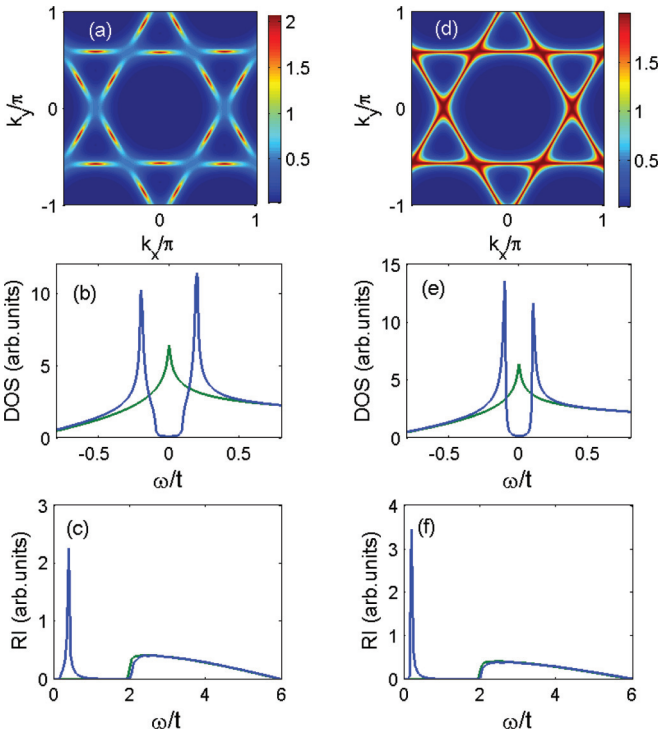

FIG. 5. (Color online) The same plot as Fig. 4 but for $\mu = t$.

$\omega = 0.2t$, below which Raman absorption is forbidden [Fig. 5(c)]. While for the extended-s-wave pairing, the DOS is zero at $-0.1t < \omega < 0.1t$ and the two van Hove singularity peaks arise at $\omega = \pm 0.1t$; therefore, the PBP is at $\omega = 0.2t$, below which there is also an energy cutoff for Raman absorption [Fig. 5(f)]. For the two pairing symmetries, beyond the Raman peak, the Raman spectra for SC graphene are similar to those in the normal state. These are understandable since the SC gap only influences the DOS around the FS, away from which the DOS is barely changed.

We have not mentioned the effect of Coulomb screening on the Raman spectrum of SC graphene. By comparison, we find that when it is not doped (at $\mu = 0$), the Raman spectrum obtained from the screened response function is the same as that obtained from the bare one. While when it is doped, for example, at $\mu = 0.5t$ and $\mu = t$ discussed above, the intensity of pair breaking peak obtained from the screened response function decreases slightly compared with that obtained from the bare one, but the positions of the peak (Raman shift) are the same for the two cases. For the high-energy Raman peak, the bare and screened Raman spectra overlap with each other, which are the same as those of the normal state graphene.[27] Experimentally, it is the screened Raman spectra that could be detected.

From the results above, we find that the Raman spectra for each pairing symmetry are different when the doping level changes, i.e., for $d + id'$-wave pairing, when it is not doped, the Raman spectrum has a low-energy kink and a high-energy Raman peak. When it is doped, there is a low-energy SC PBP, below which there is an energy cutoff. No Raman absorption is allowed below the cutoff energy, indicating a full gap. While for extended-s-wave pairing, when it is not doped, the Raman spectrum is similar to that of the normal state graphene. When it is doped, there is also a low-energy SC PBP. When the doping level increases, the low energy behavior changes from a linear line to the appearance of cutoff energy, indicating that the gap changes from nodal to full. Besides, the Raman spectra of the two pairing symmetries at the same doping level are also different. These features of Raman spectra can be used to discern the $d + id'$-wave and extended-s-wave pairings of SC graphene.

IV. CONCLUSION

In conclusion, we theoretically studied the electronic Raman response of SC graphene with two possible pairing symmetries ($d + id'$ wave and extended s wave) at half filling and different doping levels. We found that the electronic Raman spectra for each pairing symmetry behave differently when the doping level changes. At the same doping level, the Raman spectra for $d + id'$- and extended-s-wave parings are also different. From the number and position of Raman peaks, as well as the low energy Raman behavior, the two pairing symmetries can be clearly discerned.

ACKNOWLEDGMENTS

This work is supported by the National Natural Science Foundation of China (Grants No. 11104099 and No. 10974086), the Open Foundation from the National Laboratory of Solid State Microstructures (Grant No. M22010), and the Natural Science Foundation of the Educational Department of Anhui Province of China (Grants No. KJ2010B184 and No. KJ2012A252).

*luhongyan2006@gmail.com

[1] K. S. Novoselov, A. K. Geim, S. V. Morozov, D. Jiang, Y. Zhang, S. V. Dubonos, I. V. Grigorieva, and A. A. Firsov, Science **306**, 666 (2004).
[2] A. H. Castro Neto, F. Guinea, N. M. R. Peres, K. S. Novoselov, and A. K. Geim, Rev. Mod. Phys. **81**, 109 (2009).
[3] V. N. Kotov, B. Uchoa, V. M. Pereira, F. Guinea, and A. H. Castro Neto, Rev. Mod. Phys. **84**, 1067 (2012).
[4] J. L. McChesney, A. Bostwick, T. Ohta, T. Seyller, K. Horn, J. González, and E. Rotenberg, Phys. Rev. Lett. **104**, 136803 (2010).
[5] D. K. Efetov and P. Kim, Phys. Rev. Lett. **105**, 256805 (2010).
[6] N. M. R. Peres, M. A. N. Araujo, and Daniel Bozi, Phys. Rev. B **70**, 195122 (2004).
[7] T. Paiva, R. T. Scalettar, W. Zheng, R. R. P. Singh, and J. Oitmaa, Phys. Rev. B **72**, 085123 (2005).
[8] H. B. Heersche, P. Jarillo-Herrero, J. B. Oostinga, L. M. K. Vandersypen, and A. F. Morpurgo, Nature (London) **446**, 56 (2007).
[9] F. Miao, S. Wijeratne, Y. Zhang, U. C. Coskun, W. Bao, and C. N. Lau, Science **317**, 1530 (2007).
[10] X. Du, I. Skachko, and E. Y. Andrei, Phys. Rev. B **77**, 184507 (2008).
[11] A. M. Black-Schaffer and S. Doniach, Phys. Rev. B **75**, 134512 (2007).
[12] G. Profeta, M. Calandra, and F. Mauri, Nat. Phys. **8**, 131 (2012).
[13] B. Uchoa and A. H. Castro Neto, Phys. Rev. Lett. **98**, 146801 (2007).
[14] B. Kumar and B. S. Shastry, Phys. Rev. B **68**, 104508 (2003).
[15] Q.-H. Wang, D.-H. Lee, and P. A. Lee, Phys. Rev. B **69**, 092504 (2004).
[16] C. Honerkamp, Phys. Rev. Lett. **100**, 146404 (2008).
[17] S. Pathak, V. B. Shenoy, and G. Baskaran, Phys. Rev. B **81**, 085431 (2010).
[18] T. Ma, Z. Huang, F. Hu, and H.-Q. Lin, Phys. Rev. B **84**, 121410 (2011).
[19] R. Nandkishore, L. S. Levitov, and A. V. Chubukov, Nat. Phys. **8**, 158 (2012).
[20] W.-S. Wang, Y.-Y. Xiang, Q.-H. Wang, F. Wang, F. Yang, and D.-H. Lee, Phys. Rev. B **85**, 035414 (2012).
[21] M. L. Kiesel, C. Platt, W. Hanke, D. A. Abanin, and R. Thomale, Phys. Rev. B **86**, 020507 (2012).
[22] Y. Jiang, D.-X. Yao, E. W. Carlson, H.-D. Chen, and J. P. Hu, Phys. Rev. B **77**, 235420 (2008).
[23] T. P. Devereaux and R. Hackl, Rev. Mod. Phys. **79**, 175 (2007); H.-Y. Lu and Q.-H. Wang, Phys. Rev. B **75**, 094502 (2007); H.-Y. Lu, Y. Wan, X.-M. He, and Q.-H. Wang, Chin. Phys. Lett. **26**, 097402 (2009).
[24] A. M. Zhang and Q. M. Zhang, Mod. Phys. Lett. B **26**, 1230020 (2012); H.-Y. Lu, D. Wang, S. Chen, W. Wang, and P.-F. Gong, Physica C **471**, 453 (2011).
[25] A. A. Abrikosov and V. M. Genkin, Zh. Eksp. Teor. Fiz. **65**, 842 (1973) [Sov. Phys. JETP **38**, 417 (1974)].
[26] T. Strohm and M. Cardona, Phys. Rev. B **55**, 12725 (1997).
[27] H.-Y. Lu and Q.-H. Wang, Chin. Phys. Lett. **25**, 3746 (2008).